Constructing the Universe with Clusters of Galaxies, IAP 2000 meeting, Paris (France) July 2000
Florence Durret & Daniel Gerbal eds.

The multiphase nature of the intra–cluster medium of some clusters of galaxies

Massimiliano Bonamente[1] Richard Lieu[2], Jonathan P.D. Mittaz[3]
1) Osservatorio Astrofisico di Catania, Via S. Sofia 78, I-95125 Catania, Italy
2) Department of Physics, University of Alabama, Huntsville, AL 35899, U.S.A.
Mullard Space Science Laboratory, UCL, Holmbury St. Mary, Dorking, Surrey, RH5 6NT, U.K.

The discovery of EUV and soft X–ray excess emission in clusters of galaxies (the cluster soft–excess phenomenon) challenged the notion of the hot ($\sim 10^{7-8}$ K) gas as the only dominant thermal component of the intracluster medium (ICM). The spatial analysis of ROSAT PSPC 1/4 keV images presented here reveals compelling evidence for substantial amounts of cold gas (HI) in the ICM of the Coma and Virgo clusters. This finding bolsters the original interpretation of the soft excess as emission from a 'warm' ($\sim 10^6$ K) gas and points to the scenario of a multiphase ICM where the hot component co–exists with gases at sub–Virial temperatures (the 'warm' and 'cold' phases).

1 Introduction

Studies of X-ray emission from the hot intracluster medium (ICM), using the latest data and analysis methods, led many to infer that the ICM may contain various gas components considerably cooler than the Virial temperature (see, e.g., Allen 2000 and Buote et al. 1999). An important question concerns the mass budgets of the various components. Contemporaneously, a consensus is finally reached on the range of allowable values spanned by some key cosmological parameters: based on a number of independent approaches, it was shown that these parameters consistently fall within narrow windows, which, when taken altogether, suggest that most of the baryonic mass in the present day universe exist as a 10^{5-6} K gas (Cen & Ostriker 1999, Maloney & Bland-Hawthorn 1999). The discovery of excess EUV and soft X-ray emission from clusters of galaxies (Lieu et al. 1996a,b; Mittaz, Lieu, & Lockman 1998) was originally interpreted as due to substantial amounts of warm gas at temperatures of $\sim 10^6$ K. In this *paper* we present evidence for the widespread existence of even cooler gases, which bolsters the possibility of a warm intermediate phase and the notion of a multiphase ICM with sub-Virial temperature gases playing an important role in a proper understanding of clusters.

Our results are obtained by a search for signatures of spatially resolved absorption in the C-band images of the ROSAT PSPC (defined here and after as the passband between PI channels 20 and 41, or approximately 0.2 – 0.4 keV). This band is ideally suited to the detection of intervening cold ICM gas: any depletion in the background cluster emission cannot be attributed to such other possibilities as, e.g., warm absorbers. In contrast, previous inferences of the like were based on less sensitive data at higher energies (Allen 2000, White et al. 1991), and arrived

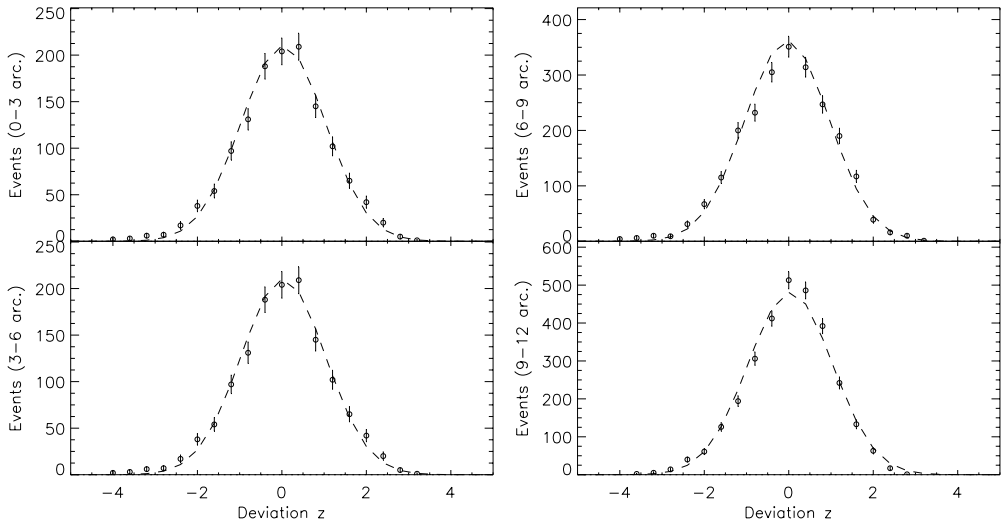

Figure 1: Spatial distribution of events for the inner annuli of a blank field centered at PSPC boresight. A $2.25' \times 2.25'$ scanning box detects, for each detector position, the deviation z between the number of enclosed counts (N) and the mean background level (μ), in units of the standard deviation σ (where z=(N-μ)/σ). The y–axis gives total number of boxes at a given deviation z and the dashed line is the best–fit profile expected from a smooth distribution, viz., a gaussian of fixed width σ=1. The gaussian mean was varied to account for any possible systematics in the background subtraction.

at values of the HI column density $\sim 10^{21}$ cm^{-2} for the centers of cooling flow clusters, values which are difficult to reconcile with the centrally peaked emissions reported by EUVE from Virgo and A1795, since EUV photons cannot possibly penetrate such large columns. The C-band also responds to small amounts of HI: for incident radiation from a plasma of 0.5 solar abundance and temperatures kT = 0.1 and 5.0 keV, reminiscent of the warm and hot ICM, an optical depth in the C-band corresponds to cold gas of HI column density $N_H \sim 1.3 \times 10^{20}$ and 1.7×10^{20} cm^{-2}, respectively. Moreover, at high Galactic latitudes the absorption of C-band extragalactic emission by our interstellar medium is not very severe, so that data of good statistical quality are available for the brighter clusters.

2 Method of analysis

The method we adopted is to evaluate the spatial smoothness of the soft excess from two clusters, using PSPC C-band images. The first step consists of estimating the hot gas contribution to the C-band fluxes. To accomplish this, the cluster diffuse emission was divided into concentric annuli and spectra in the R47 band (a terminology often used to denote PI channels 42-201, or energies 0.4 – 2.0 keV) was modelled with a photoelectrically absorbed thin plasma emissivity code (MEKAL in XSPEC), where temperature (T) and elemental abundances (A) were fitted to the data (see Table 1). In the R47 band, in fact, any contributions from a 'warm' gas are minimal, and this modelling returns a spatially resolved measurement of the hot ICM parameters. At each radius r, the best-fit model defines a ratio $f(r)$ of the C-band to R47 count rates; removal of the hot ICM contribution from the C-band is obtained via the equation

$$c_{res} = c - f(r) \times h\,, \tag{1}$$

where c and h are respectively the background subtracted C-band and R47 images.[a] The distribution of the C-band residuals, c_{res}, reveals regions of soft excess (positive values) as well as

[a] Since azimuthal symmetry is assumed, $f(r)$ is a radially symmetric 'image' of the C-to-R47 conversion factor described in the text.

regions of absorption (negative values). For the Coma cluster, a similar technique was adopted, whereby PSPC spectra were succesfully modelled with a photoelectrically absorbed MEKAL code with T and A fixed at the best-fit Ginga measurements (T=8.21 keV, A=0.21 solar, Hughes et al. 1993). Given that the central region of the cluster is sufficiently isothermal, the ratio f(r) is a constant function of radius.

Table 1: Best–fit parameters for the hot ICM of Virgo; errors are 90% confidence (χ^2 + 2.701 criterion).

Region (arcmin)	Temperature (keV)	Abundance	red. χ^2 (d.o.f)
0–3	$1.47\ \pm^{0.05}_{0.04}$	$0.46\ \pm^{0.03}_{0.04}$	1.15(156)
3–5	$2.03\ \pm^{0.12}_{0.13}$	$0.55\ \pm^{0.09}_{0.08}$	1.25(156)
5–7	$2.42\ \pm^{0.24}_{0.19}$	$0.45\ \pm^{0.09}_{0.07}$	1.2(156)
7–10	$2.53\ \pm^{0.21}_{0.22}$	$0.39\ \pm^{0.07}_{0.08}$	1.1(156)
10–15	$2.49\ \pm^{0.19}_{0.19}$	$0.33\ \pm^{0.06}_{0.08}$	1.29(156)
15–19	$3.14\ \pm^{0.42}_{0.34}$	$0.37\ \pm^{0.11}_{0.10}$	1.07(156)

After removal of the hot ICM contribution, a box of size $2.25' \times 2.25'$ scans the residual image area (c_{res} in the notation of Eq. 1), stepping its center by 0.25 arcmin at a time. The box size was chosen to ensure sufficient enclosed counts for normal distribution of Poisson fluctuations. Then, if a background subtracted image is smooth, its mean brightness should be zero and deviations about the mean should follow a fixed gaussian. This, a consequence of the central limit theorem, was confirmed by our own simulations as well as C-band images of blank fields. As an example, we show in Figure 1 the results for various annuli of a blank field within the central PSPC area; the data were acquired during a 30 ksec pointing to a celestial direction where the Galactic N_H is $\sim 1.4 \times 10^{21}$ cm^{-2} (RA=50.29^o, DEC=40.74^o, RP number 800034a01). The C-band sky background is low, due to its anti–correlation with HI, yet the forementioned box size still yielded an average of ~ 40 counts per box, so that gaussian statistics apply.

When we apply the method to a cluster field, the X-ray emission is often not smooth to begin with. Deviations from the azimuthally averaged surface brightness for a R47 image of Coma are shown in Fig. 2a (see later for details on the observation): the image clearly reveals substructures. Nonetheless our method of analysis remains meaningful, because such regions of anisotropy do not correspond to a different spectral hardness when compared with the surroundings (i.e. the same conversion factor f applies when subtracting the hot ICM contribution to the C-band flux). Further, the lack of any resemblance between the soft excess and X-ray images, as we demonstrate by Fig. 2b, confirms that any spatial structures in the former are due to emission or absorption of the soft cluster flux. For the Virgo cluster, similar results hold, with the exception of three strong absorption features detected towards the cluster center, which are positionally coincident with enhancements of the X-ray (0.4-2 keV) emission. These regions are the subject of a separate spectral analysis in the following section.

3 The Virgo and Coma clusters

The central region of the Virgo cluster is dominated by the giant galaxy M87; near the center of Coma are likewise located the cluster's two brightest supergiant elliptical galaxies (NGC 4874 and NGC 4889) and a few discrete X–ray sources. We therefore excluded from analysis the innermost portions of the two clusters (angular radii $\leq$ 3 arcmin). We show in Figure 3 the C-band soft–excess image smoothness evaluation for the region between radii of 3 and 15 arcmin, centered at M87, and divided into 4 annuli. The dataset is from the ROSAT archive (observation

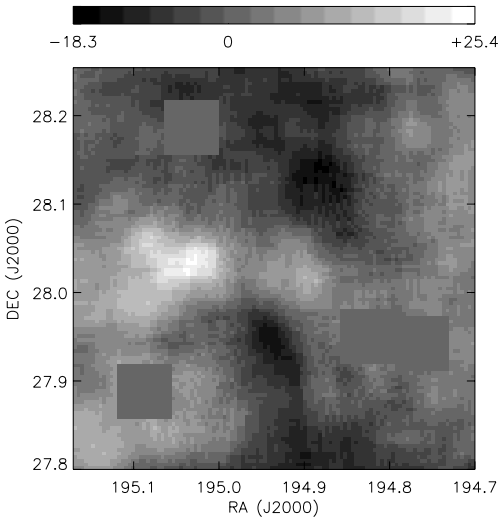

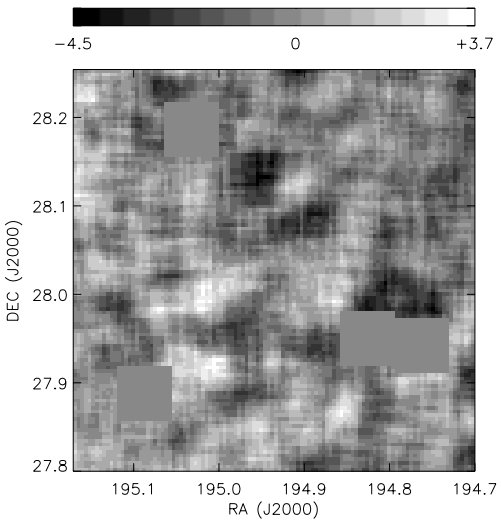

Figure 2: (a) At each detector position, a $2.25' \times 2.25'$ scanning box detects the difference between the number of enclosed R47 counts and the azimuthally averaged value at that radius, in units of the standard deviation (see caption of Fig. 1). (b) C-band residual image of Coma: same scanning box detects, at each detector position, the deviation between the number of enclosed counts and 0, the mean expected value in the absence of absorption or soft excess emission. Unit of measure is the standard deviation σ. The σ-scale of 2(b) is set to reveal the absorption features responsible for the left tail of Figure 3; these features are clearly not positionally coincident with any emission features of the hot ICM, as is evident from a comparison of 2(a) with 2(b). Regions containing obvious point sources were excluded from the analysis (gray boxes).

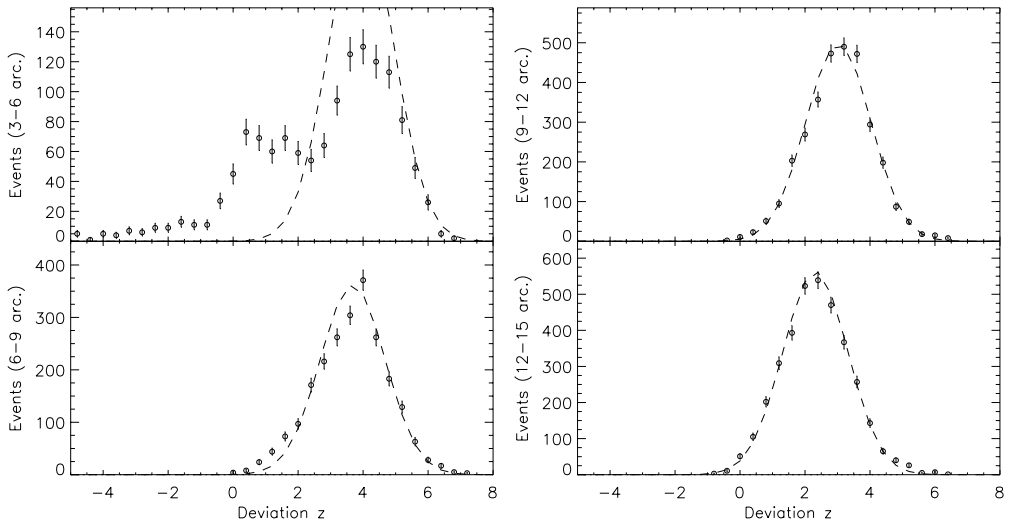

Figure 3: Spatial distribution of events for the central region of the Virgo cluster. As in Fig. 1, dashed line gives the best–fit model for a smooth distribution (i.e. one–gaussian) except that it fails to account for the data here. Annular radii are measured from the position of M87, which is at PSPC boresight.

number RP8000365). Significant departures from gaussian behavior, clearly noticeable within a radius of 9 arcmin, are in the form of an asymmetric extension to the left, which is symptomatic of absorption features resolved by the scanning box[b]. Indeed the features within 6 arcmin radius are obviously identifiable in the image.

Table 2: Performance of the two–gaussian model for the Virgo cluster, where μ_1 and μ_2 are the means of the two gaussians, each having fixed width at σ=1; $\Delta\chi^2$ is the χ^2 reduction from the one–gaussian fit, and the covering factor is obtained by the ratio of the normalization constants. Errors are 90 % confidence (χ^2+ 2.701 criterion). The outermost annulus does not require a second (left) gaussian.

Region (arcmin)	μ_1	μ_2	cov. factor	χ^2(d.o.f)	$\Delta\chi^2$
3–6	0.93±0.09	$4.1\pm^{0.06}_{0.05}$	0.34±0.02	67.6(26)	594.4
6–9	$2.27\pm^{0.15}_{0.13}$	$3.27\pm^{0.04}_{0.05}$	0.16±0.02	19.4(17)	76.4
9–12	$1.7\pm^{0.4}_{0.25}$	3.07±0.03	0.042±0.019	31.5(16)	7.5
12–15	2.32±0.017	–	–	42.8(18)	–

A simple 'partial covering' model to interpret the observations assumes that for each annulus inwards of 12 arcmin, a certain fraction of its area (which can be broken into smaller, disjointed areas) has emission uniformly shadowed by foreground intrinsic HI, as illustrated in Fig. 4. Then the distribution of soft emission is the sum of two gaussians: their peak positions contain information about the mean brightness in the absence of intrinsic absorption and the HI column for the absorbed areas. Moreover, the relative normalization of the gaussians converts to a partial covering factor. In Figure 5 we show the performance of this model for one of the Virgo annuli, and in Table 2 the best-fit parameters of the model are listed for all the regions. The decreasing trend of the covering factor points to a radially declining influence of absorption *by clouds within the cluster*. We emphasize that despite its success as indicated by the $\Delta\chi^2$ values when compared with a single gaussian fit (Table 2), the model may still be over-simplistic because the absolute

[b] Emission features, including any residual radial surface brightness gradients not removed by the subtraction of C-band radiation from the hot ICM, would have been manifested as *right* extension tails, which are evidently absent.

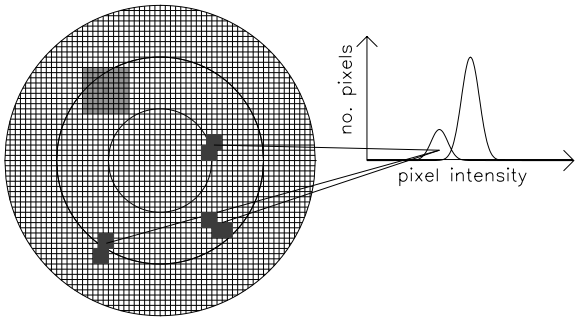

Figure 4: The scanning box (light grey) can detect silhouettes (dark grey) of the surface brightness which are responsible for the bimodal behavior of the spatial distribution of events (see e.g. Fig. 4 and Fig. 7).

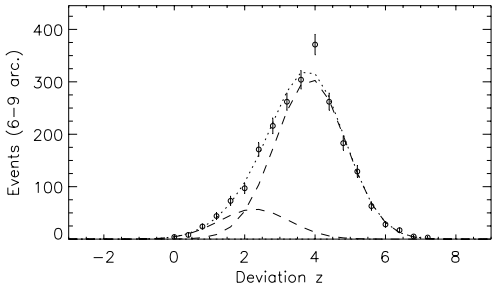

Figure 5: Fitting the distribution of events in the 6–9 arcmin annulus of Virgo with the two–gaussian 'partial covering' model. A significant improvement over one gaussian is achieved (see also Table 1). The positive mean of the right (main) gaussian revelas soft–excess emission.

χ^2 values do not imply acceptability. Indeed, additional spatially unresolved absorption may well be present, and the effect of foreground cluster emission may well have caused an underestimate of the HI towards these central radii. It is also possible that the column density of HI clouds is not uniform; nonetheless the quality of present data does not warrant more sophisticated models, for this purpose one must await observations by the XMM/EPIC instrument.

In Figure 6 we show the three deepest absorption features which exist in the innermost area; they are positionally coincident with prominent radio lobes (Harris et al. 1999) and with enhancements in the X–ray (0.5–2 keV) emission, see Böhringer et al. (1995), whose study led to the proposition of a lower temperature for the hot ICM in the radio lobes than in the surrounding regions. The forementioned enhancement was then interpreted as due to a Fe line feature at $\sim$ 1 keV. We accordingly examined spectra for two regions, one including one feature to the east and the other to the south-west of M87. Since similar results apply to both regions, here we focus on the eastern knot: Figure 7a shows that a photo-absorbed MEKAL code with T=1.3 and A=0.45 (as in Böhringer et al. 1995) can in fact model the observed spectrum (χ^2=188 for 155 degrees of freedom, with a null probability of 3.6 %). It is however not physically obvious why radio features (symptomatic of relativistic particles) are positionally coincident with a temperature decrease in the hot gas. An alternative explanation of the C-band flux reduction would invoke cold gas (HI): we therefore attempted to model the two regions using

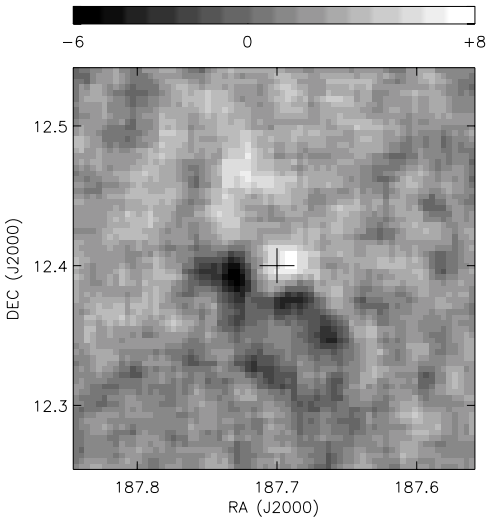

Figure 6: C–band soft excess image of Virgo, in units of statistical significance σ of signals within a $2.25' \times 2.25'$ scanning box centered at each pixel position. The deep absorption features to the south of M87 (cross) are coincident with the location of radio lobes (Harris et al. 1999).

the best-fit hot ICM parameters for their corresponding annulus (T=1.47 keV, A=0.46 solar, see Table 1): the eastern knot shows a -7σ decrement from the model in the 0.2-0.4 keV band (fig. 7b), yet if the total absorption was allowed to vary we could obtain a good fit (χ^2=165 for 154 degrees of freedom, null probability of 25 %). The extra absorption required above the Galactic line-of-sight column is $N_H \sim 4.5\times10^{19}$ cm^{-2} for a region ~ 2 square arcmin in size. A possible interpretation is that the high pressure of relativistic particles can lead to compression of the hot gas trapped inside the radio lobes to high density, with consequent rapid cooling to very low temperatures. The evidence for depleted emission in other regions of the cluster (Fig. 3), as well as in the Coma cluster (see below), strengthens our present scenario, because none of those are caused by the subtraction of spatially corresponding enhancements in the hot ICM radiation.

Table 3: Two–gaussian model for the Coma cluster, see caption of Table 1.

Region (arcmin)	μ_1	μ_2	cov. factor	χ^2(d.o.f)	$\Delta\chi^2$
3–6	3.16±0.06	5.3±0.084	0.58±0.03	15.7(16)	302.8
6–9	1.35±0.08	3.5±0.045	0.32±0.02	50(21)	379.8
9–12	0.14±0.15	1.85±0.04	0.14±0.027	10.4(17)	85.4
12–15	1.05±0.08	–	–	21(14)	–

A similar analysis of PSPC C–band data of the Coma cluster (archival identification RP800005) proved equally fruitful. The spatial distribution of the emission is clearly not smooth, see Fig. 8. The use of a two–gaussian 'partial covering' model results in significant improvement of the

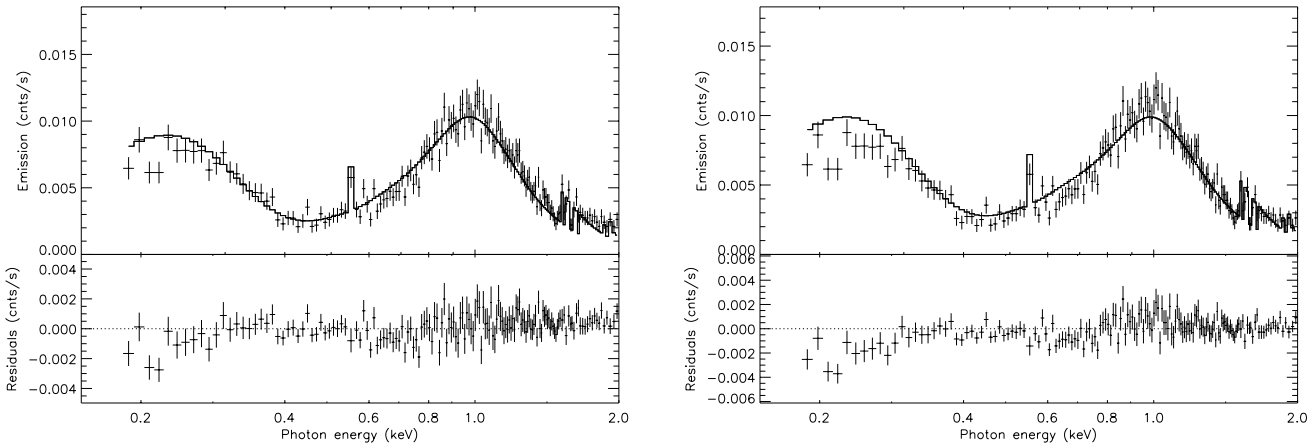

Figure 7: (a) PSPC spectrum of a ~ 2 square arcmin region encompassing the 'absorption feature' to the east of M87 (cross), fitted to a MEKAL code with the parameters of Böhringer et al. (1995). (b) same PSPC spectrum when only PI channels 42-201 ($\sim 0.4 - 2$ keV) are fitted to a MEKAL code with the best-fit parameters of the 0-3 arcmin annulus (see Table 1).

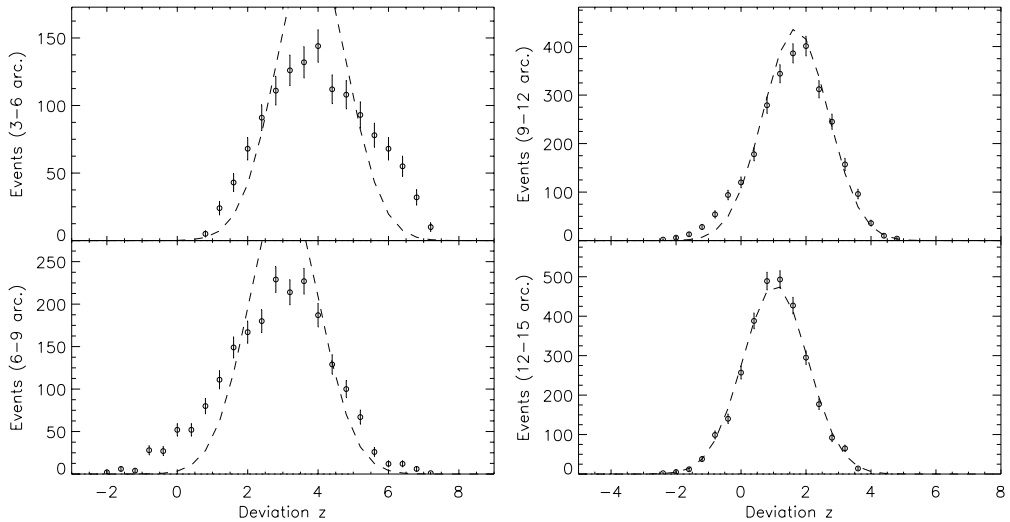

Figure 8: Event distribution for the Coma cluster (see caption of Fig. 3); the dashed line is the best–fit single gaussian model, as before. The center of our annular system is at the X–ray centroid of Coma, which is near boresight. The positive mean of the right gaussian reveals soft excess emission.

Table 4: HI column density ($N_{\rm H}$) and mass estimates for the Coma and Virgo clusters. The peak positions of the two gaussians (Tables 1 and 2) are first transformed to units of flux, and then, using the absorption cross–section of Morrison and McCammon (1983), the flux difference is converted to $N_{\rm H}$. The tabulated mass refers to the total value for the lines of sight within each annular region as $M = N_{\rm H} \times (area) \times (c.f.) \times m_{\rm H}$, where $c.f.$ is the covering factor of the region as from Tables 1 and 2.

Cluster	region (arcmin)	$N_{\rm H}$ (cm^{-2})	mass ($M_\odot$)
Virgo	3–6	3.5×10^{19}	3.4×10^{8}
"	6–9	3×10^{19}	2.4×10^{8}
"	9–12	6×10^{19}	1.7×10^{8}
Coma	3–6	1.4×10^{19}	3.8×10^{9}
"	6–9	1.5×10^{19}	4×10^{9}
"	9–12	1.7×10^{19}	1.8×10^{9}

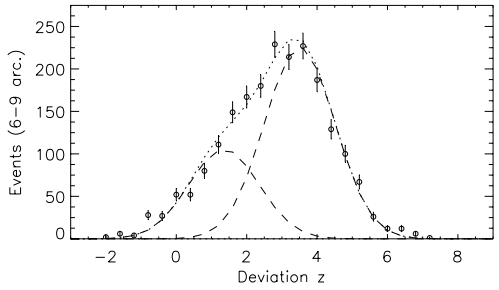

Figure 9: Use of the 'partial covering' model for the 6–9 annulus of Coma brings considerable improvement to the fit (see also Table 2).

goodness–of–fit (see Table 3), where the decrease of the covering factor with radius points again to a centrally peaked distribution of absorbers; the outermost annulus (12–15 arcmin) in fact does not require a second gaussian. As an example, the performance of the two–gaussian model for the 6–9 arcmin region is shown in Fig. 9. This result is of particular importance as Coma is the first non–cooling flow cluster which exhibits evidence for cold gas clouds.

4 Discussion and conclusions

The adopted method of analysis affords us estimates of column densities and HI mass for the two clusters, see Table 4. Could this absorption be caused by line–of–sight cluster galaxies? Rich clusters of galaxies, such as Virgo and Coma, are known to have a large fraction of gas–poor elliptical and S0 galaxies, and only a small fraction of late type galaxies (such as spirals). Moreover, cluster galaxies show an HI deficit when compared to field galaxies of same morphology, especially toward the central regions (e.g. Huchtmeier and Richter 1986; Dickey 1997). In the case of Virgo a simple galaxy count for the 3–12 arcmin region from M87 (using the NED database) revealed only three known, early type member galaxies along the line of sight, which is too few in number to account for the absorption features of Fig. 6. Likewise, a recent 21-cm line investigation of the Coma cluster with the VLA array (Bravo–Alfaro et al. 2000) detected no galaxies with HI content above $\sim 10^8$ M$_\odot$, the typical detection limit of that survey, in the central 10 arcminutes. Within the context of a galaxy origin of the cold gas, this is again inconsistent with our HI estimates in Table 4.

It is far more plausible that the reported effect is due to intracluster HI which might have, at least in part, been released to the intergalactic space by ram pressure stripping. Cold gas masses

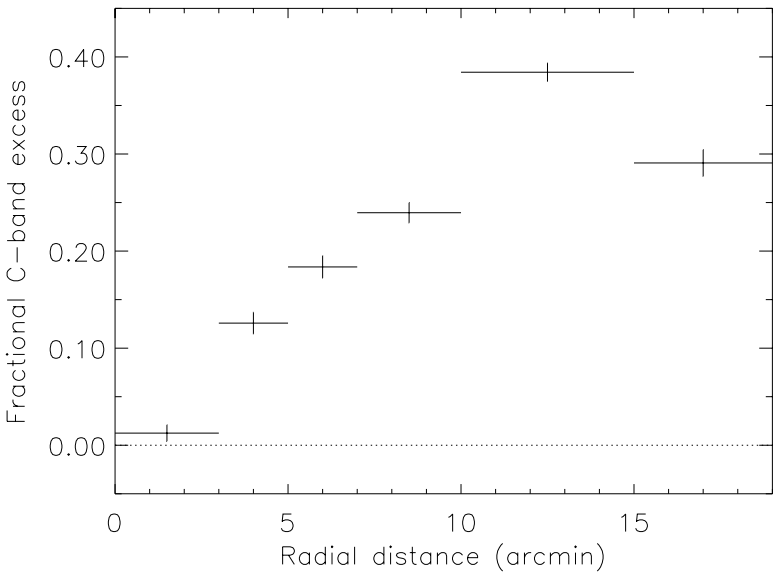

Figure 10: The 'soft-excess radial trend' effect of the Virgo cluster, illustrated by a plot against cluster radius of the soft X-ray fractional excess η, defined as $\eta = (p - q)/q$, where for a given annulus p is the observed C–band flux after subtracting the sky background, and q is the expected flux from the hot ICM as determined by fitting the PI channels 50 – 200 ($\sim$ 0.5 – 2.0 keV) using the MEKAL thin plasma emission code (Mewe, Lemen and van den Oord 1986; Mewe, Gronenshild and van den Oord 1985; Kaastra 1992) and Galactic absorption according to Morrison & McCammon (1983).

of the order $10^{9-11} M_{\odot}$ contribute to only a small fraction of the cluster's total baryonic mass, the latter of order a few $\times 10^{12} M_{\odot}$ for Virgo (see, e.g., Bahcall and Sarazin 1979) and a few $\times 10^{14} M_{\odot}$ for Coma (Briel, Henry and Böhringer 1992). Such ratios are in general agreement with current cosmological models (see e.g. Maloney and Bland–Hawthorn 1999; Cen and Ostriker 1999), which predict that baryons at the present epoch reside mostly in a warm ($\sim 10^{5-6}$ K) gas and much less so as hot ($\sim 10^{7-8}$ K) and cold ($\leq 10^5$ K) gases.

We note that the phenomenon of the soft excess radial trend (meaning rising importance of the soft component with radius), known to exist in the clusters A1795 (Mittaz, Lieu and Lockman 1998) and A2199 (Lieu et al. 1999), was recently interpreted as indicative of centrally peaked intrinsic cluster absorption (Lieu, Bonamente and Mittaz 2000). As shown in Figure 10, this effect is also present in the C–band excess of Virgo, and may indeed be due to the gradual disappearance of absorption with increasing radius reported in Table 4.

The co–existence of a cold phase and hot ICM components raises questions concerning *if* and *where* an intermediate warm phase is present. The evidence for cold HI presented in this *paper* reinforces the thermal interpretation of the cluster soft–excess syndrome: some warm gas can certainly be generated at the interface between the cold and hot gases, e.g. by the 'mixing layer' mechanism (Fabian 1997). The emerging scenario is a three–phase ICM, where the hot gas emits the bulk of the X–ray emission, and the warm gas is responsible for the soft–excess emission. The cooler gas (T $\leq 10^5$ K), found by our spatial smoothness test, causes substantial reduction of EUV and soft X–ray fluxes in some locations, and the soft excess radial trend detected in the C band of Virgo (see Fig. 10) could then be due to the absorption effect of a centrally peaked distribution of HI.

Acknowledgments

This is where one places acknowledgments for funding bodies etc. Note that there are no section numbers for the Acknowledgments, Appendix or References.

References

1. S.W. Allen, *MNRAS accepted* , (2000).
2. J.N. Bahcall and C.L. Sarazin *ApJ* **213**, L99 (1977).
3. H. Böhringer, P.E.J. Nulsen, R. Braun and A.C. Fabian 1995, *MNRAS* **274**, L67 (1995).
4. H. Bravo–Alfaro, V. Cayatte, J.H. Van Gorkom and C. Balkowski, *AJ* **119**, 580 (2000).
5. U.G. Briel, J.P. Henry and H. Böhringer, *A&A* **259**, L31 (1992).
6. D.A. Buote, C.R. Canizares and A.C. Fabian, *MNRAS* **310**, 483 (1999).
7. R. Cen and J.P. Ostriker, *ApJ* **514**, 1 (1999).
8. J.M. Dickey, *AJ* **113**, 1939 (1997).
9. A.C. Fabian, *Science* **113**, 48 (1997).
10. D.E. Harris, F. Owen, J.A. Biretta and W. Junor, *Proceedings of the Ringberg Workshop on Diffuse Thermal and Relativistic Plasma in Galaxy Clusters* **MPE Report 271**, 111 (1999).
11. W.G. Huchtmeier and O.G. Richter, *A&A* **64**, 111 (1986).
12. J.P. Hughes, J.A. Butcher, G.C. Stewart and Y. Tanaka 1993, *ApJ* **404**, 611 (1993).
13. J.S. Kaastra, *An X-Ray Spectral Code for Optically Thin Plasmas* **Internal SRON-Leiden Report, updated version 2.0**, (1992).
14. R. Lieu, J.P.D. Mittaz, S. Bowyer, F.J. Lockman, C.-Y. Hwang and J.H.H.M. Schmitt 1996a, *ApJ* **458**, L5 (1996a).
15. R. Lieu, J.P.D. Mittaz, S. Bowyer, J.O. Breen, F.J. Lockman, E.M. Murphy and C.-Y. Hwang,1996b, *Science* **274**, 1335 (1996b).
16. R. Lieu, M. Bonamente, J.P.D. Mittaz, F. Durret, S. Dos Santos and J.S. Kaastra, 1999, *ApJ* **527**, L77 (1999).
17. R. Lieu, M. Bonamente and J.P.D. Mittaz 2000, *A&A submitted* , (2000).
18. P.R. Maloney and J. Bland-Hawthorn, *ApJ* **522**, L81 (1999).
19. R. Mewe, E.H.B.M. Gronenschild, and G.H.J. van den Oord, *A&A Supp.* **62**, 197 (1985).
20. R. Mewe, J.R. Lemen, and G.H.J. van den Oord, **A&A Supp. 65**, 511 (1986).
21. xiJ.P.D. Mittaz, R. Lieu, F.J. Lockman, *ApJ* **498**, L17 (1998).
22. R. Morrison and D. McCammon, *ApJ* **270**, 119 (1983).
23. D.A.White, A.C. Fabian, R.M. Johnstone, R.F. Mushotzky and K.A. Arnaud, *MNRAS* **252**, 72 (1991).